Optical-frequency-comb generation with collinear acousto-optic diffraction: Theory and simulations

Sergey N. Mantsevich*
M.V. Lomonosov Moscow State University, 1 Leninskie Gory, Moscow 119991, Russia

Andrey S. Voloshin
Russian Quantum Center, 45 Skolkovskoye shosse, Moscow, 121353, Russia

Konstantin B. Yushkov
National University of Science and Technology "MISIS", 4 Leninsky Prospekt, Moscow 119049, Russia

(Received 16 April 2019; published 16 July 2019)

Optical frequency combs (OFCs) are of extreme importance for modern photonics. A great number of OFC generation methods and practical application ideas have been suggested. In this paper we propose and theoretically analyze an OFC generation method based on frequency-shifting loop utilizing collinear acousto-optic (AO) diffraction. This method offers two OFC generation schemes. The first one applies the closed-loop optical system with collinear AO cell driven by external radio-frequency (rf) generator. The second scheme applies a principle of an optoelectronic oscillator. This system includes not only the optical feedback but also the optoelectronic feedback connecting the optical output of the system with the piezoelectric transducer of the AO cell and operates above the self-excitation threshold without external rf generator. In both cases OFCs may be obtained in several ways: two different types of single side band modulation and amplitude modulation. The switching between the methods is realized by mutual reorientation of a pair of polarizers placed in front of and behind the AO cell and achromatic half-wave plate included in the optical feedback loop. It is shown that the parameters OFCs obtained in the system with only optical feedback are determined by AO cell material, rf generator signal frequency and magnitude, optical loss and amplification. The system with both optic and electronic feedback gives the unique opportunity to obtain chirped OFCs even without using any rf generator. In this case the OFC parameters depend on the AO cell material, electric feedback gain, optical loss, and optical gain.

DOI: 10.1103/PhysRevA.100.013829

I. INTRODUCTION

Optical frequency combs (OFCs) have revolutionized optical measurements and are still one of the most important breakthroughs in photonics in recent years. OFCs represent a train of ultrashort laser pulses that corresponds to an optical spectrum of equally spaced frequencies, thousands of narrow teeth [1]. Such combs have become key tools in optical precision measurements [2], next-generation telecommunication networks [3], molecular spectroscopy [4], distance ranging [5], dual-comb spectroscopy [6], and definition of the SI second [7,8]. First OFC sources were developed for the near-infrared (NIR) spectral range, while frequency combs centered in the visible (VIS), ultraviolet (UV), or midinfrared (MIR) are in great demand [7–13].

There are various techniques for optical comb generation depending on the particular application. The first optical comb generators were based on femtosecond lasers and they gave rise to the active study of comb applications outside of pure optical frequency metrology. The main disadvantage of such combs is the tooth spacing defined by the length of the laser cavity with typical values from 10 MHz–1 GHz. But there are some important applications that require much higher line spacing, for example, astronomical spectrograph calibration [9] or optical telecommunications based on DWDM [3,14]. Generation of Kerr soliton combs, so-called, soliton microcombs, paves the way to compact OFC generators based on nonlinear microresonators with ultrahigh Q factor [15–17] and allows fully on-chip integration [18,19]. Kerr combs provide line spacing from 1 GHz–1 THz defined by microresonator radius [20,21].

New physical principles are being actively studied for generating OFC [22,23]. New methods based on semiconductor and quantum cascade lasers [24,25], cavity electromagnetically induced transparency [26], titanium-indiffused lithium-niobate waveguide resonators [27], quantum dots [28] have been proposed. Another approach that has been proposed to produce OFCs from a CW laser combines gain switching and optical injection locking in a semiconductor laser [29,30]. This method makes it possible to achieve dual-comb generation (potentially from visible to midinfrared), although the spectra thus obtained are still limited to tens of lines.

Another widely used technique for OFC synthesis is based on the frequency shifting of a CW laser using electro-optic, acousto-optic (AO), or single side band modulators inside the loop with optical feedback [31–39], so-called, frequency-shifting loop (FSL). OFC generated in FSL based on electro-optical modulator is called an electro-optic comb. This approach paves the way to tunable comb generator, i.e., making

*Corresponding author: snmantsevich@yahoo.com

tunable both the central frequency and the comb spacing. The line spacing is defined by the radio-frequency (rf) function generator driving the modulators and may vary from MHz to tens of GHz. The comb position and the span are defined by the pump CW laser and the gain range of the optical loop. It is important to note that electro-optic comb is constructed with off-the-shelf fiber and optical components that makes them convenient tools for various applications, including characterization and generation of other frequency combs and optical signals [40,41]. Electro-optic combs are perfectly suited for dual-comb spectroscopy since coherence of two combs may be achieved by a single laser pumping two optical loops [42–44]. Electro-optic dual-comb technique measuring broadband optical waveforms at ultrahigh single-interferogram refresh rates (up to 25 MHz) has been demonstrated recently [45]. While OFC based on electro-optical modulators are widely used, acousto-optic device based OFCs are faintly studied. However, acousto-optic OFCs have a high potential for some applications. Acousto-optic OFC was utilized for multiheterodyne spectroscopy with high spectral resolution [46]. New concepts for photonic generation of broadband optical combs, consisting of relatively flat spectra with >1000 modes and providing tunable linear rf chirp rate, are proposed [47].

In this paper we analyze generation of OFCs in a FSL scheme based on acousto-optic diffraction in collinear geometry utilizing its properties as a modulator and frequency shifter [48–50]. Applying these features in conventional optical scheme with single frequency CW laser seeded into an optical FSL with an amplifier provides new regimes of optical comb generation. AO diffraction in a collinear filter enables controlled interference between the diffraction orders, and different parameters of OFC generation can be obtained. The CW laser seeds the first optical frequency that is shifted and amplified in the optical loop. We characterized operation regimes in dependence on different parameters, AO filter operation, gain, optical polarization in different parts of the scheme. Then we propose a technique for OFC generation utilizing additional optoelectronic feedback that eliminates the need of any rf signal generator and AO cell drive. The comb span is limited by the AO filter transfer function and the optical amplifier bandwidth. Also, the generated comb has an important property, in particular, comb spacing is linearly increasing. Linear chirped OFCs are in high demand in various applications [47]. The proposed optical scheme significantly simplifies the generation of chirped OFC.

The paper is organized as follows. In Sec. II we describe collinear AO diffraction with different settings of input and output polarizers and possible architectures of the OFC generator based on it. Phenomenological model of OFC generation is observed in Sec. III, and the analytical model followed by resulting simulations is presented in Sec. IV.

II. SYSTEM ARCHITECTURE

A. Collinear AO filter

Collinear geometry of AO interaction in crystals takes place when wave vectors of ultrasound and incident and diffracted optical waves are collinear. Most often, calcium molybdate ($CaMoO_4$) and lithium niobate ($LiNbO_3$) crystals are used for collinear AO filters [51–54]. The conventional scheme of collinear AO cell application for optical radiation spectral filtration is presented in Fig. 1. The AO cell is mounted between two linear polarizers. The angle of the input polarizer transmission axis α is chosen along one of the crystal optical eigenmodes. In the common case of collinear diffraction along one of the crystal symmetry axes, e.g., Y, the eigenmodes are polarized along other crystallographic axes, X and Z. Since the AO diffraction is accompanied by the optical polarization change to the orthogonal one, the polarizer mounted after the AO cell should have the transmission axis orthogonal to the input polarizer separating the diffracted optical beam from the incident one.

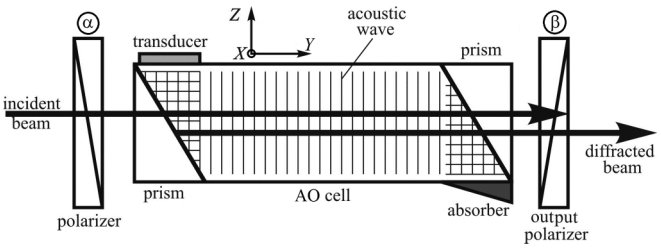

FIG. 1. Collinear AO filter in $LiNbO_3$ with arbitrary rotated input and output linear polarizers.

The relationship between ultrasound frequency f_c and wavelength λ of the optical radiation diffracted in the acoustic field is defined by the phase matching condition for the collinear AO diffraction:

$$f_c(\lambda) = \frac{V}{\lambda}|n_e - n_o|, \tag{1}$$

where V is the acoustic wave velocity, n_o and n_e are the ordinary and extraordinary refractive indices of the AO crystal. Thus, varying the acoustic frequency, we are able to select different spectral components of the optical signal. For a $LiNbO_3$ collinear AO filter $V = 3940$ m/s, $n_o = 2.211$ and $n_e = 2.138$ at $\lambda = 1.55$ μm resulting in $f_c = 185.6$ MHz.

Plane wave interaction is considered as a first approximation to describe AO diffraction [55]. It describes well the diffraction of collimated laser beams [56]. Each component of the electromagnetic field can be characterized by its polarization **e**, frequency ω, and complex amplitude C. In the case corresponding to Fig. 1, the Bragg AO diffraction is described by the couple-mode equations for the complex amplitudes of the electromagnetic field components $C^X(y)$ and $C^Z(y)$ on the interval $y \in [0, l]$:

$$\frac{dC^X}{dy} = -\frac{\Gamma}{2l}\exp\left(-j\frac{R}{l}y + j\Phi\right)C^Z;$$
$$\frac{dC^Z}{dy} = \frac{\Gamma}{2l}\exp\left(j\frac{R}{l}y - j\Phi\right)C^X, \tag{2}$$

where $R = (2l\pi/V)(f - f_c)$ is the phase mismatch depending on the frequency f; $\Gamma = (2\pi/\lambda)l\Delta n$ is the Raman-Nath parameter; Δn is the maximum variation of the crystal

refractive index under the action of the acoustic wave; Φ is the ultrasonic phase; l is the AO interaction length. The superscript hereinafter denotes polarization of the electromagnetic field component. The general solution of Eq. (2) at $y = l$ is

$$C^X(l) = \exp\left(-j\frac{R}{2}\right)\left[C^X(0)\cos\frac{A}{2} + \frac{jRC^X(0) - \Gamma\exp(j\Phi)C^Z(0)}{A}\sin\frac{A}{2}\right];$$
$$C^Z(l) = \exp\left(j\frac{R}{2}\right)\left[C^Z(0)\cos\frac{A}{2} - \frac{jRC^Z(0) - \Gamma\exp(j\Phi)C^X(0)}{A}\sin\frac{A}{2}\right], \quad (3)$$

where $A = \sqrt{\Gamma^2 + R^2}$.

Acousto-optical interaction is linear with respect to light, therefore Eq. (2) can be equivalently analyzed in the spectral domain. Another consequence of linearity is that a broad optical spectrum can be diffracted by a multifrequency ultrasound without phase mismatch [57–59]. This feature is used to generate a broadband OFC as discussed in Sec. IV C.

We assume that the polarizers' orientations are defined by angles α and β with respect to Z axis. For the conventional collinear AO filter the incident light polarization is chosen in accordance with the crystal eigenmode polarizations, and two polarizer settings are possible: $\alpha = 0^\circ$ and $\beta = 90^\circ$ (extraordinary wave of the input) or $\alpha = 90^\circ$ and $\beta = 0^\circ$ (ordinary wave at the input). It has been shown that the conventional collinear filter is only the one of the variants that may take place in the system of two polarizers and collinear AO cell between them [48–50]. In the general case of incident optical radiation having arbitrary linear polarization, the light radiation at the AO cell output consists of four components polarized along X and Z axes of the crystal. These components are described at the AO cell output by the following equations:

$$E_0^X = E_\mathrm{i}\sin\alpha\left(\cos\frac{A}{2} - j\frac{R}{2}\operatorname{sinc}\frac{A}{2\pi}\right)\times\exp\left[j\left(\omega_0 t - k_\mathrm{e} l + \frac{R}{2}\right)\right];$$
$$E_{+1}^Z = -E_\mathrm{i}\sin\alpha\frac{\Gamma}{2}\operatorname{sinc}\frac{A}{2\pi}\times\exp\left\{j\left[(\omega_0+\Omega)t - k_\mathrm{o} l - \frac{R}{2}\right]\right\};$$
$$E_0^Z = E_\mathrm{i}\cos\alpha\left(\cos\frac{A}{2} + j\frac{R}{2}\operatorname{sinc}\frac{A}{2\pi}\right)\times\exp\left[j\left(\omega_0 t - k_\mathrm{o} l - \frac{R}{2}\right)\right];$$
$$E_{-1}^X = E_\mathrm{i}\cos\alpha\frac{\Gamma}{2}\operatorname{sinc}\frac{A}{2\pi}\times\exp\left\{j\left[(\omega_0-\Omega)t - k_\mathrm{e} l + \frac{R}{2}\right]\right\}, \quad (4)$$

where E_i is the incident wave electromagnetic field, $\Omega = 2\pi f$, ω_0 is the frequency of input optical radiation, and $k_\mathrm{o} = 2\pi n_\mathrm{o}/\lambda$, $k_\mathrm{e} = 2\pi n_\mathrm{e}/\lambda$. The components of the electromagnetic field $E_{-1}^X(y,t)$ and $E_{+1}^Z(y,t)$ are Doppler shifted. In the case of AO diffraction in $LiNbO_3$, the shift is positive for diffraction from X to Z component and negative otherwise.

Passing through the output polarizer rotated at the angle β with respect to Z axis, the field components acquire the same polarization and interfere. The resulting intensity after the output polarizer is

$$I_\mathrm{d} = \left|\left(E_0^Z + E_{+1}^Z\right)\cos\beta + \left(E_0^X + E_{-1}^X\right)\sin\beta\right|^2. \quad (5)$$

In the general case, the intensity I_d can be written as the sum of three components with amplitudes depending on the mutual orientation of the polarizers [48–50]:

$$I_\mathrm{d} = I_0 + I_1\cos(\Omega t + \phi + \Phi) + I_2\cos(2\Omega t + \phi + 2\Phi), \quad (6)$$

where ϕ is the additional phase shift appearing at collinear AO interaction. In the conventional variant of AO collinear filter, I_0 component that we will call the constant component acquires the maximum magnitude:

$$I_0 = I_\mathrm{i}\frac{\Gamma^2}{4}\operatorname{sinc}^2\left(\frac{A}{2\pi}\right), \quad (7)$$

where I_i is the incident light intensity. The maximum of I_0 is achieved when $\Gamma = \pi$ and $R = 0$. Simultaneously, I_1 and I_2 are equal to zero. In the conventional variant only one of $E_{-1}^X(y,t)$ and $E_{+1}^Z(y,t)$ components exists after the output polarizer depending on the polarization of incident optical radiation.

The component I_1 reaches the maximum for either $\alpha = 0^\circ$ or $\alpha = 45^\circ$ and $\beta = \alpha + 45^\circ$. The I_1 dependence on system parameters and time is described by the following equation:

$$I_1(t) = I_\mathrm{i}\frac{\Gamma}{4}\operatorname{sinc}\left(\frac{A}{2\pi}\right)\sqrt{4\cos^2\left(\frac{A}{2}\right) + R^2\operatorname{sinc}^2\left(\frac{A}{2\pi}\right)} \times\cos(\Omega t + \phi + \Phi). \quad (8)$$

The I_1 component exists due to the interference between the zeroth and the first diffraction orders. There are two spectral components at the output, one with the frequency of initial radiation and the second with the Doppler-shifted frequency. The component I_2 for such mutual orientation of polarizers equals to zero, but the I_0 component in this geometry always equals to a half of incident light intensity, so it is not convenient to use this geometry for the optical radiation filtration applications. A distinctive feature in this case is that the light intensity varies in time with the ultrasound frequency f. The I_1 magnitude achieves the maximum when $\Gamma = \pi/2$.

The I_2 component is produced by the interference of $E_{+1}^Z(y,t)$ and $E_{-1}^X(y,t)$ components. So two diffracted components exist at the optical output and both of them are Doppler shifted but in the opposite directions. The maximum of the I_2 component is achieved when $\alpha = \beta = 45^\circ$. If the I_2 component is used, the intensity at the system output is

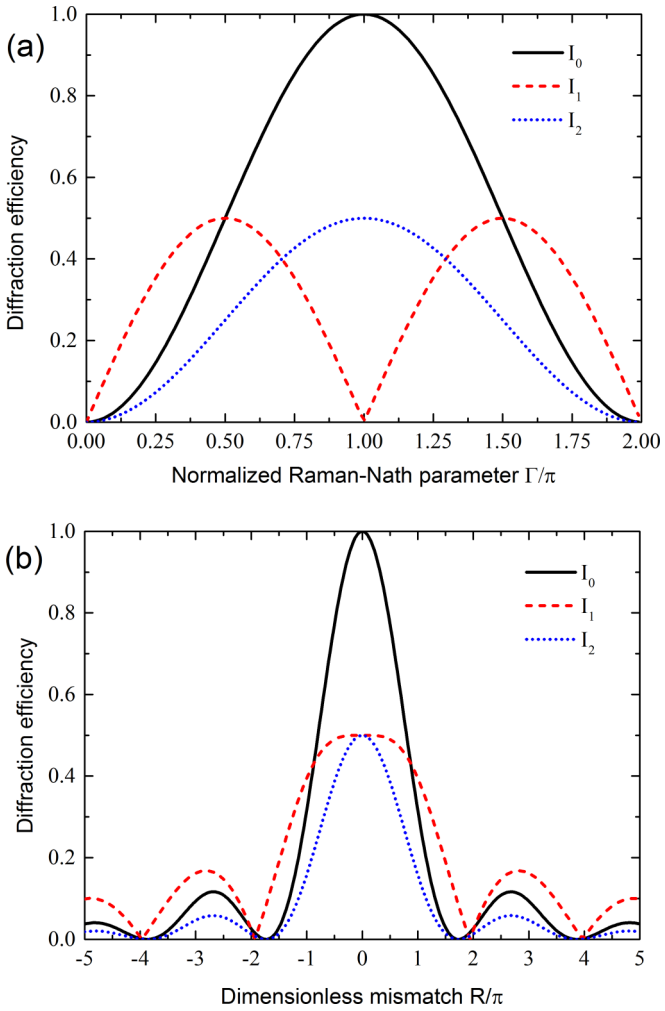

FIG. 2. (a) Diffraction efficiency and (b) transmission functions for the I_0, I_1, and I_2 components of collinear AO diffraction.

modulated in time with doubled ultrasound frequency:

$$I_2(t) = I_i \frac{\Gamma^2}{8} \operatorname{sinc}^2\left(\frac{A}{2\pi}\right) \cos(2\Omega t + \phi + 2\Phi). \quad (9)$$

The I_2 component achieves the maximum when $\Gamma = \pi$. The constant component is not equal to zero in this case also. But unlike the case of the I_1 component, the constant component varies with mismatch R. So the second harmonic I_2 is the most inconvenient for practical applications.

The most interesting case of mutual orientation of the polarizers takes place when the I_1 component magnitude is maximal. Modulation of light intensity with the ultrasound frequency makes it possible to create an electric feedback circuit. The frequency-modulated I_1 component is detected by a photodetector and the amplified electrical signal feeds the AO cell transducer [60,61].

Calculated values of each component of the output optical beam are represented in Fig. 2. The calculations were obtained setting $\alpha = 0^\circ$ and $\beta = 90^\circ$ for I_0 component, $\alpha = 0^\circ$ and $\beta = 45^\circ$ for I_1 component, and $\alpha = 45^\circ$ and $\beta = 90^\circ$ for I_2 component.

Figure 2(a) represents the dependencies of AO diffraction efficiency I_p/I_i $(p = 0, 1, 2)$ on the Raman-Nath parameter Γ that is proportional to the amplitude of the acoustic wave in the AO cell. A useful feature of the I_1 component is that the maximum diffraction efficiency for it is achieved at twice lower Γ value than for the other components, which means four times less power of ultrasound. Maximum values of I_1 and I_2 components are $0.5I_i$ because there is also a constant component $I_0 = 0.5I_i$. Thus, both I_1 and I_2 provide 100% amplitude modulation of the light radiation at the system output [49,50].

The dependencies of AO diffraction efficiency on the dimensionless mismatch R are represented in Fig. 2(b). These dependencies may be treated as the transmission functions of the AO device [48,49]. The transmission functions for the constant component and the second harmonic are the same but for the factor of 2. The I_1 component has a specific shape with a flat top and relatively high side lobes. The pass band of the system is 1.7 times wider in this case than for I_0 and I_2 components.

B. Closed-loop optical system

The Doppler shift of diffracted light at the output of the AO cell can be used to create an OFC from single-frequency laser radiation in a FSL [31,35,39]. Similar to previously reported OFC generators based on AO devices (AOM and AOFS), a collinear AO filter is placed into the FSL to obtain the optical comb.

The distinctive feature of the proposed optical system is the collinear geometry of AO diffraction. Commonly, if the comb is generated by multiple successive amplitude modulation of the light beam intensity, then the standing acoustic wave AO modulator is used as the main element of the FSL [32]. If the comb is obtained by SSB modulation, then the main element is either a tunable AO filter or an AOFS [39]. The application of noncollinear AO devices raises the problem of angular dispersion since the diffraction angle varies with optical wavelength and ultrasound frequency. Compensation for deflection of the diffracted beam requires a special analysis and cannot be full in a general case [62]. Angular dispersion is one of the main limiting factors of OFC bandwidth generated by means of noncollinear AO devices. Using a collinear AO filter ensures that all spectral components propagate strictly along the same direction and can be coupled to the fiber FSL with minimum losses.

A closed-loop optical setup with a collinear AO filter is shown in Fig. 3. The laser with $\lambda = 1.55$ μm optical radiation wavelength is used as the master oscillator. The laser radiation is inserted into the polarization maintaining optical fiber and passes through the 2×2 fiber coupler. The optical collimator is connected to one of the coupler outputs. The optical beam emerged from the collimator passes through a polarizer rotated at the angle α to Z axis of the AO crystal.

Ultrasound is excited in the AO cell with the rf generator connected to the piezoelectric transducer. In a general case, the acoustic frequency f is not equal to the collinear AO diffraction phase matching frequency f_c for the given optical wavelength. The optical radiation is diffracted by the acoustic wave and passes through the output polarizer oriented at angle

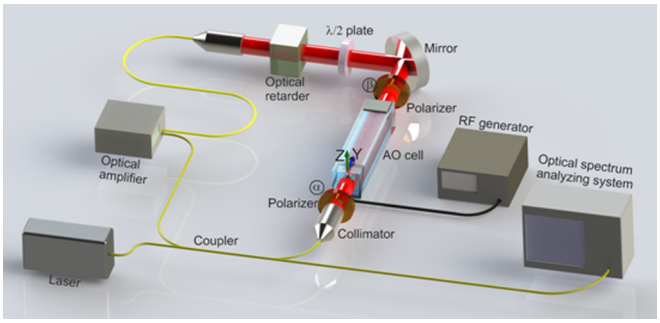

FIG. 3. Scheme of closed-loop optical system for OFC generation with a collinear AO filter.

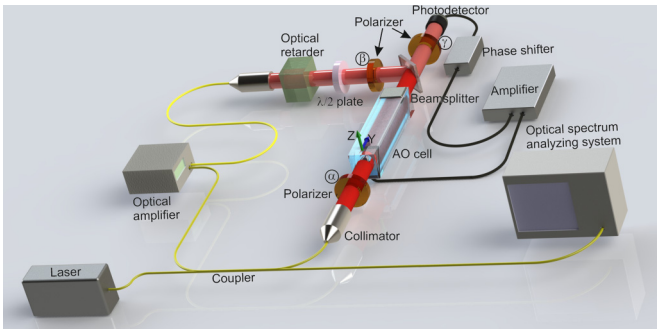

FIG. 4. Scheme of closed-loop optical system for OFC generation with a collinear AO filter and both optical and electronic feedback.

β with regard to Z axis. The components of the electromagnetic field can be found from Eq. (4) and the intensity follows Eq. (5).

An achromatic half-wave plate (HWP) is mounted after the polarizer. It is used to make the output beam polarization the same as the incident one. An optical phase retarder may be mounted after the HWP to compensate for the optical beam phase shift if needed. The phase shift may appear when light passes through the optical feedback loop and also as a result of AO diffraction. Then, through the collimator, the light radiation is fed into the optical amplifier and goes to the second input of the coupler. The seed laser radiation is mixed with the radiation passed through the FSL. The second output of the fiber coupler is off loop and can be used for measurement.

The peculiarities of collinear AO diffraction with arbitrary polarizer settings described in Sec. II A provide the possibility to generate optical combs applying SSB modulation (with either I_0 or I_1 component) as well as applying amplitude modulation with ultrasound frequency (with I_2 component). Switching between modulation modes is performed simply rotating the polarizers and the HWP. One should set $\alpha = 0^\circ$, $\beta = 90^\circ$ and the HWP should rotate the light polarization by 90° to obtain SSB modulation with I_0 component. SSB modulation with I_1 component is obtained by setting $\alpha = 0^\circ$, $\beta = 45^\circ$ and the HWP should rotate the light polarization by 45°. Amplitude modulation with ultrasound frequency is takes place when the polarizers' orientation is the same, $\alpha = \beta = 45^\circ$, and for this reason one does not need the HWP.

C. Closed-loop optical system with optoelectronic feedback

It has been recently demonstrated that the AO system consisting of a collinear AO cell and an optoelectronic feedback may operate as the acousto-optic generator [63–66]. The principle of electronic feedback can be applied to generate OFCs with higher performance. Novel architecture of the OFC generator based on a collinear AO filter and a dual feedback is shown in Fig. 4.

The second feedback circuit connects the optical output of AO cell with its piezoelectric transducer. The mirror at the AO cell output is replaced with a beam splitter having the splitting ratio ϵ. This beam splitter should be mounted before the output polarizer [67]. One of the beams from the beam splitter is sent to the optical feedback loop, and the second one is fed to the electrical feedback circuit. After the beam splitter, the second optical beam passes through the polarizer rotated at the angle γ relatively to the Z axis of the AO filter. The polarizer must be oriented in such a way that the light beam at its output obtains the amplitude modulation with the ultrasound frequency (maximum of I_1 component). Modulated optical radiation enters the photodetector with sensitivity ρ that transforms it into electric signal with the frequency equal to the frequency of the light beam amplitude modulation. It is the same frequency that the ultrasound wave excited in AO cell has. The signal from the photodetector passes through the feedback circuit with gain κ. The feedback consists of a phase shifter and a rf amplifier to fulfill the phase and amplitude balance conditions [60,61,67,68]. The output of the feedback circuit is connected to the AO cell piezoelectric transducer having efficiency ψ.

At the certain gain magnitude determined by the electric feedback parameters and the incident light radiation intensity, the system overcomes the self-excitation threshold [65,66]. In this case, the system can operate without an external rf generator. The acoustic wave with frequency f_c determined by the incident optical radiation wavelength Eq. (1) will be excited in the AO cell. Thus, as many acoustic frequencies will be excited in the AO cell as the components with intensities higher than necessary for self-excitation at a given gain exist in the spectrum of the incident optical radiation [66].

As the result, we obtain an optoelectronic system with two feedback loops: an optical one needed to increase the number of components in the spectrum of light radiation, and an optoelectronic one, which is required for the diffraction of these optical components in the AO cell. The AO interaction bandwidth has no contribution to the bandwidth of the optoelectronic system in the generation mode, i.e., when the electrical gain is high enough [66].

In practice, the bandwidth is limited by technical noises (e.g., dark current of the photodetector, the seed laser noise, and spontaneous emission in the optical amplifier) and inhomogeneous temperature distribution in the AO crystal resulting in broadening of the AOTF frequency response. However, appearance of each line in the OFC is accompanied by appearance of a new phase matched line in the rf spectrum. Thus, each spectral component of the OFC is diffracted with zero mismatch, independently of the others, at its own acoustic frequency.

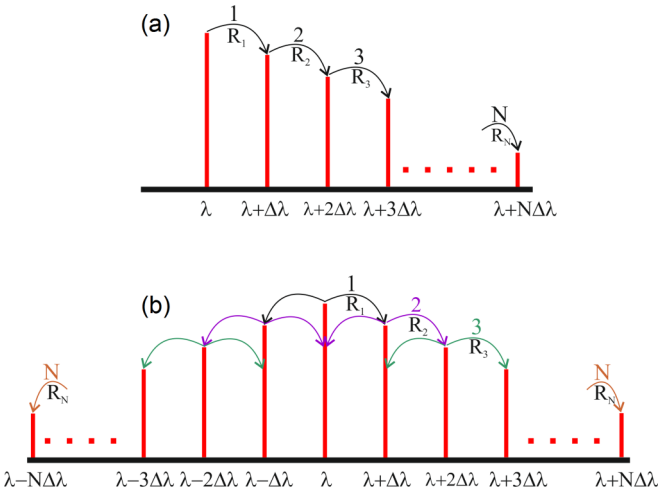

FIG. 5. The process of OFC generation for (a) SSB modulation with I_0 or I_1 components and (b) amplitude modulation with I_2 component in closed-loop system.

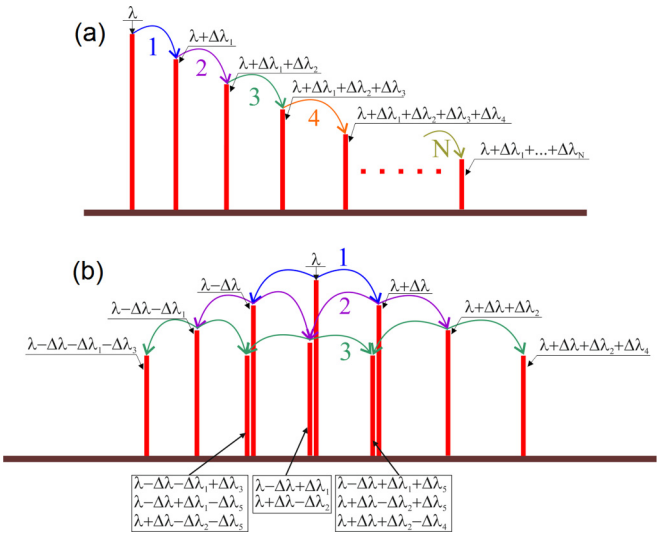

FIG. 6. The process of OFC generation in the system with two feedback loops for (a) SSB modulation with I_0 or I_1 components and (b) amplitude modulation with I_2 component.

III. QUALITATIVE EXAMINATION

A. Equally spaced OFC

The peculiarities of collinear AO diffraction described in Sec. II A provide the possibility to generate OFC's in various ways. The possible cases are SSB modulation with either I_0 or I_1 component or amplitude modulation with ultrasound frequency using I_2 component. Wherein the switching between modulation modes is performed simply by rotating the polarizers and the HWP.

The appearance of new components in the optical radiation spectrum of after N passes through the FSL is schematically shown in Fig. 5. Figure 5(a) illustrates the optical comb generation process applying SSB modulation with either I_0 or I_1 component. The additional spectral components appear in this case due to the change of the light radiation wavelength caused by the Doppler effect, which takes place in the case of light diffraction by the traveling acoustic wave. The comb appears from sequential diffraction of light by the same single-frequency ultrasonic wave, wherein the diffracted beam at the nth pass through the optical feedback loop is the incident light for the $(N+1)$th pass. Thus, the spectral interval between the OFC components is determined by the frequency of rf generator. In the process of diffraction in $+1$st or -1st diffraction order, the wavelength of the next spectral component is less or more than the previous one. The choice of the diffraction order is determined by the orientation of the input polarizer ($\alpha = 0^\circ$ for -1st order and $\alpha = 90^\circ$ for $+1$st order).

The performance of the OFC generator has principal differences in the cases of using I_0 and I_1 components. In the case of the constant component, I_0, only one component of electromagnetic field exists after the output polarizer. As follows from Eq. (7), all spectral components have the same phase. In the case of SSB modulation realization with I_1, two components are observed at the output and their interference causes the appearance of the phase shift between the adjacent spectral components of the comb Eq. (8). The second difference is that for I_1 component we need four times lower ultrasonic power consumed by the AO cell than for the constant component [see Fig. 2(a)].

The disadvantage of the SSB modulation method is that the subsequent spectral components are obtained only by diffraction of the previous ones. Consequently, the spectral width of the comb will be small due to the presence of optical loss and high spectral selectivity of the collinear AO interaction. Figure 5(b) illustrates the optical comb generation using the successive light intensity modulation with I_2 component. In this case, each spectral component is modulated by magnitude with the frequency of ultrasound beam excited in the AO cell and produces two new spectral components. In this case, the magnitude of each component is influenced by two adjacent components. The phase shift between adjacent OFC components exists, as follows from Eq. (9). The value of this shift for the Nth spectral component is defined as $\phi_N + \Phi$ where Φ depends on the acoustic wave parameters and $\phi_N = R_N + (k_e - k_o)l$, where R_N is the acousto-optic mismatch for Nth component.

B. Chirped OFC

The next case is OFC generation in the AO system with both optical and electrical feedback loops. Similar to the case of a single FSL system described above, one may use SSB modulation with I_0 or I_1 components or amplitude modulation at the ultrasound frequency applying I_2 component.

Figure 6 schematically shows the appearance of new components in the OFC spectrum after N passes through the optical feedback loop. Figure 6(a) illustrates generation of an optical comb using SSB modulation, using either I_0 or I_1 component. In this case, additional spectral components appear due to a change in the wavelength of the light radiation caused by the Doppler frequency shift. Thus, if seed laser radiation with a wavelength λ polarized along Z axis is fed to the optical input, then if the third polarizer is oriented at an angle $\gamma = 45^\circ$ and the gain κ is greater than the excitation

threshold, oscillations with a frequency $f_1 = V|n_e - n_o|/\lambda$ will occur in the electric feedback circuit. Then an acoustic wave with frequency f_1 will be excited in the AO cell and, for example, if the light is diffracted to the -1st order, the optical wavelength will be shifted by $\Delta\lambda_1 = \lambda^2 f_1/(c + f_1\lambda)$. Therefore, in the FSL with the orientation of the second polarizer at an angle $\beta = 90^\circ$, the light radiation with the wavelength $\lambda + \Delta\lambda_1$ will exist. Passing through the HWP light will acquire the same polarization as at the input of the AO cell.

During the second pass of light through the system two spectral components with wavelengths λ and $\lambda + \Delta\lambda_1$ and the same polarizations exist at the input. The presence of two components in the optical radiation spectrum causes the emergence of two ultrasound frequencies in the feedback circuit f_1 and f_2 and two acoustic frequencies in the AO cell. The optical wave with the wavelength λ is diffracted by the first of them and $\lambda + \Delta\lambda_1$ by the second. In this process the optical waves with the wavelength $\lambda + \Delta\lambda_1$ and $\lambda + \Delta\lambda_1 + \Delta\lambda_2$ appear. Assuming that $|n_e - n_o| = \text{const}$. (that is correct for lithium niobate crystal in a wide range in the IR region) the spectral interval $\Delta\lambda_N$ between two components with numbers N and $N - 1$ is defined by the following equation:

$$\Delta\lambda_N = \lambda \frac{V|n_e - n_o|c^{N-1}}{(c - V|n_e - n_o|)^N}. \tag{10}$$

It follows from Eq. (10) that the interval between adjacent OFC spectral components increases with number N linearly. Thus, the resulting OFC is linearly chirped and we are able to obtain this chirp even without using an external rf generator like it was done in Ref. [47]. The optical wavelength of the Nth OFC spectral component that appears after the Nth pass of the optical beam through the FSL is defined as:

$$\lambda_N = \lambda \left(\frac{c}{c - V|n_e - n_o|} \right)^N. \tag{11}$$

The dependence of the interval between adjacent com teeth, $\Delta\lambda_N$, on the wavelength of the Nth tooth, λ_N was calculated taking into consideration the dispersion of the lithium niobate refractive indices. The presented calculation results shown in Fig. 7 for the 95 nm optical band confirm the fact that the spectral interval between the components of the comb increases linearly with increasing the wavelength.

If the OFC is obtained applying I_2 component [Fig. 6(b)] due to the amplitude modulation of light intensity, two spectral components appear after the first pass of light through the FSL. These components are shifted from the central one by $\pm\Delta\lambda = \Delta\lambda_1$. At the second pass, each of the existing components is diffracted independently in the AO cell by its own acoustic wave and originate two new components. An interesting point is that the component with the wavelength $\lambda - \Delta\lambda + \Delta\lambda_1$ produced by $\lambda - \Delta\lambda$ has the same wavelength as component $\lambda + \Delta\lambda - \Delta\lambda_2$ produced by the $\lambda + \Delta\lambda$ component and the wavelength of these two new components is slightly shorter than the wavelength of initial wave λ. Thus, after the second pass of light through the system six spectral components will exist at the optical output. If we let the light to pass through the system one more time than the number of OFC components will increase to ten, and three of them will

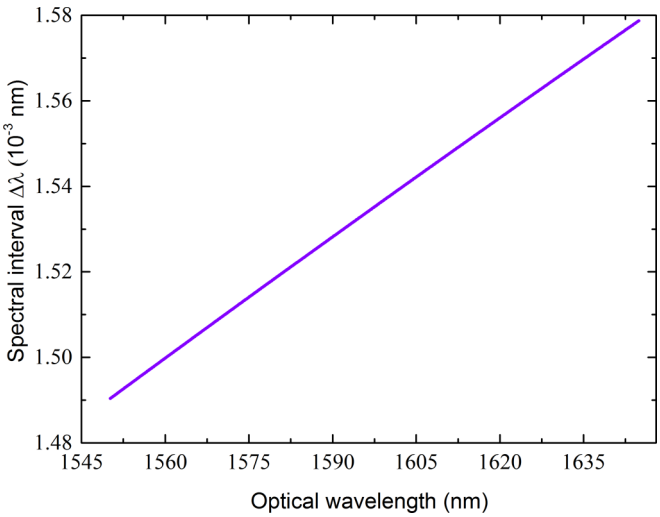

FIG. 7. The dependence of spectral interval between adjacent OFC components on optical wavelength.

obtain wavelengths close to λ and $\lambda \pm \Delta\lambda$. Comparing the OFC spectra presented in Figs. 6(a) and 6(b) it is possible to conclude that the OFC generation applying SSB modulation with I_0 component seems to be more preferable due to the absence of additional spectral components and zero phase shift between the spectral components.

IV. MATHEMATICAL MODEL AND SIMULATION RESULTS

A. Basic relations

Based on the general considerations, we introduce the mathematical model of OFC generation in the examined closed-loop systems. Analysis of the OFC generation can be performed in spectral domain. The seed laser emission is assumed to have the only frequency ω_0 in the spectrum. The OFC spectrum is expressed in a general form as sum:

$$\widetilde{\mathbf{E}}(\omega) = \mathbf{e} \sum_m S_m \delta(\omega - \omega_m), \tag{12}$$

where $\widetilde{E}(\omega)$ denotes the Fourier transform of $E(t)$; δ is the Dirac delta function; $\omega_m = \omega_0 + m\Omega$.

We normalize the fields so that the spectrum of the master oscillator used as a seed is $\widetilde{E}_{\text{seed}} = 1$. After N passes through the optical feedback system the spectrum is $\widetilde{E}_{[N]}$, so the input to the AO filter at the $(N + 1)$th pass is

$$\widetilde{\mathbf{E}}' = 0.5(\widetilde{E}_{[N]} + \widetilde{E}_{\text{seed}})\mathbf{e}_\alpha, \tag{13}$$

where $\mathbf{e}_\alpha$ is the polarization unit vector than makes an angle α with Z axis. Thus, the magnitudes of the input spectral components are

$$\begin{aligned} S'_{m,[N]} &= 0.5S_{m,[N]}, \quad m \neq 0; \\ S'_{0,[N]} &= 0.5(S_{0,[N]} + 1), \quad m = 0. \end{aligned} \tag{14}$$

We may rewrite Eqs. (4), in Fourier domain for the components of the diffracted spectrum in the following way:

$$\widetilde{E}^X_0 = \sin\alpha \sum_m S'_{m,[N]}\left(\cos\frac{A_m}{2} - j\frac{R_m}{A_m}\sin\frac{A_m}{2}\right) \times \exp\left(-jk_e l + \frac{R_m}{2}\right)\delta(\omega-\omega_m);$$

$$\widetilde{E}^Z_{+1} = -\sin\alpha \sum_m S'_{m-1,[N]}\frac{\Gamma}{A_{m-1}}\sin\frac{A_{m-1}}{2} \times \exp\left(-jk_o l - \frac{R_{m-1}}{2}\right)\delta(\omega-\omega_m);$$

$$\widetilde{E}^Z_0 = \cos\alpha \sum_m S'_{m,[N]}\left(\cos\frac{A_m}{2} + j\frac{R_m}{A_m}\sin\frac{A_m}{2}\right) \times \exp\left(-jk_o l - \frac{R_m}{2}\right)\delta(\omega-\omega_m);$$

$$\widetilde{E}^X_{-1} = \cos\alpha \sum_m S'_{m+1,[N]}\frac{\Gamma}{A_{m+1}}\sin\frac{A_{m+1}}{2} \times \exp\left(-jk_e l + \frac{R_{m+1}}{2}\right)\delta(\omega-\omega_m), \quad (15)$$

where $A_m = \sqrt{\Gamma^2 + R_m^2}$, $\omega_m = \omega_0 + m\Omega$, $R_m = (2l\pi/V)(f - f_{cm})$. Frequency f_{cm} is the AO phase matching frequency for mth OFC spectral component.

Each mth monochromatic component of the diffracted field is determined by only one of the components of the incident field having the index either $(m+1)$ or $(m-1)$. After the output polarizer, the spectrum is calculated as:

$$\widetilde{E}_{\text{out}} = \left(\widetilde{E}^Z_0 + \widetilde{E}^Z_{+1}\right)\cos\beta + \left(\widetilde{E}^X_0 + \widetilde{E}^X_{-1}\right)\sin\beta. \quad (16)$$

Equation (16) is the spectral analog of Eq. (5). Finally, we obtain

$$\widetilde{E}_{[N+1]} = \upsilon(1-\chi)\sigma\widetilde{E}_{\text{out}}, \quad (17)$$

where υ is the optical coupler coupling ratio, χ is the optical loss in the system, and σ is the gain of the optical amplifier.

In a general case, each coefficient $S_{m,[N+1]}$ in a series representation Eq. (12) of $E_{[N+1]}$ is determined by three coefficients: $S_{m-1,[N]}$, $S_{m,[N]}$, and $S_{m+1,[N]}$.

B. Equally spaced OFC

An equally spaced OFC can be obtained with optical only FSL in a system described in Sec. II B. We study different OFC generation modes in this system.

The simplest way to obtain an OFC is to apply SSB modulation with I_0 component. In this case only, it is possible to derive an analytical expression describing the process of OFC spectral components appearance at the multiple light passing through the system.

The orientation of polarizer planes in this case is chosen to be $\alpha = 0^\circ$ and $\beta = 90^\circ$. So, at the first pass at the system optical input we have $\widetilde{E}_{\text{seed}} = 1$ with polarization along Z axis and only $\widetilde{E}^X_{-1}$ exists after the output polarizer:

$$\widetilde{E}^X_{-1} = \upsilon\widetilde{E}_{\text{seed}}\cos\alpha\sin\beta\frac{\Gamma}{2}\operatorname{sinc}\frac{A_1}{2\pi} \times \exp\left(-jk_e l + \frac{R_1}{2}\right)\delta(\omega-\omega_1), \quad (18)$$

where $R_1 = (2l\pi/V)(f - f_{c1})$.

Electromagnetic spectrum at the optical feedback output after the first pass equals to:

$$\widetilde{E}_{\text{out}} = \upsilon(1-\chi)\sigma\widetilde{E}_{\text{seed}}\cos\alpha\sin\beta\frac{\Gamma}{2}\operatorname{sinc}\frac{A_1}{2\pi} \times \exp\left(-jk_e l + \frac{R_1}{2}\right)\delta(\omega-\omega_1). \quad (19)$$

Applying Eqs. (13) and (17) recurrently it is possible to obtain relation describing the OFC spectrum after N passes of light through the system:

$$\widetilde{E}_{[N]} = \widetilde{E}_{\text{seed}}\sum_{n=1}^{N}[\upsilon(1-\chi)\sigma]^n\left(\frac{\Gamma}{2}\right)^n\prod_{m=1}^{n}\operatorname{sinc}\left(\frac{A_m}{2\pi}\right). \quad (20)$$

It is easy to notice that the optical spectrum at the system output contains as many spectral components as many passes through the optical feedback loop we have. The magnitude of these components depends on the optical losses in the system, optical amplification and transmission function shape, see Fig. 2(b).

The results of the calculations carried out with Eq. (20) are presented in Fig. 8. Both the OFC spectrum and the AO filter transmission function plots are shown. At the simulations we assume that $\upsilon = 0.5$, $\chi = 0.3$, $\Gamma = \pi$, and the seed radiation wavelength of master oscillator is $\lambda = 1.55$ μm. The evaluations were carried for the case when phase-matching condition was fulfilled $R = 0$ [Figs. 8(a) and 8(b)] and for the case when R is not equal to zero [Figs. 8(c) and 8(d)].

The optical comb shape simulation fulfilled for the case when $f = f_c$ (185.6 MHz), polarizer and analyzer orientations $\alpha = 0^\circ$ and $\beta = 90^\circ$ is presented in Fig. 8(a). The simulation was done for optical gain $\sigma = 2.98$. The total width of the optical comb is only 0.45 nm. The number of spectral components in the comb is about 300 at -50 dB level. For such mutual orientation of the polarizers the diffraction occurs to the -1st order, so the optical wavelength increases with the OFC spectral component number. Spacing between the components equals to f_c. If we choose $\alpha = 90^\circ$ and $\beta = 0^\circ$ [Fig. 8(b)] the light is diffracted into the $+1$st order and we obtain the OFC symmetrical to that presented in Fig. 8(a), but the optical wavelength decreases with the OFC component number.

The optical comb shape simulations carried out for the cases $f \neq f_c$ are presented in Figs. 8(c) and 8(d). The optical comb shape spectrum contains a local minimum and an additional maximum that does not correspond to the phase matching frequency. The total spectral width of the comb increases with R growth. If $R = -2$ ($f = 185.9265$ MHz) the OFC contains 450 components and occupy 0.67 nm spectral band, the spacing between components equals to the frequency f. The optical comb shape simulation carried out for the mismatch $R = -3.5$ ($f = 185.9025$ MHz) is presented

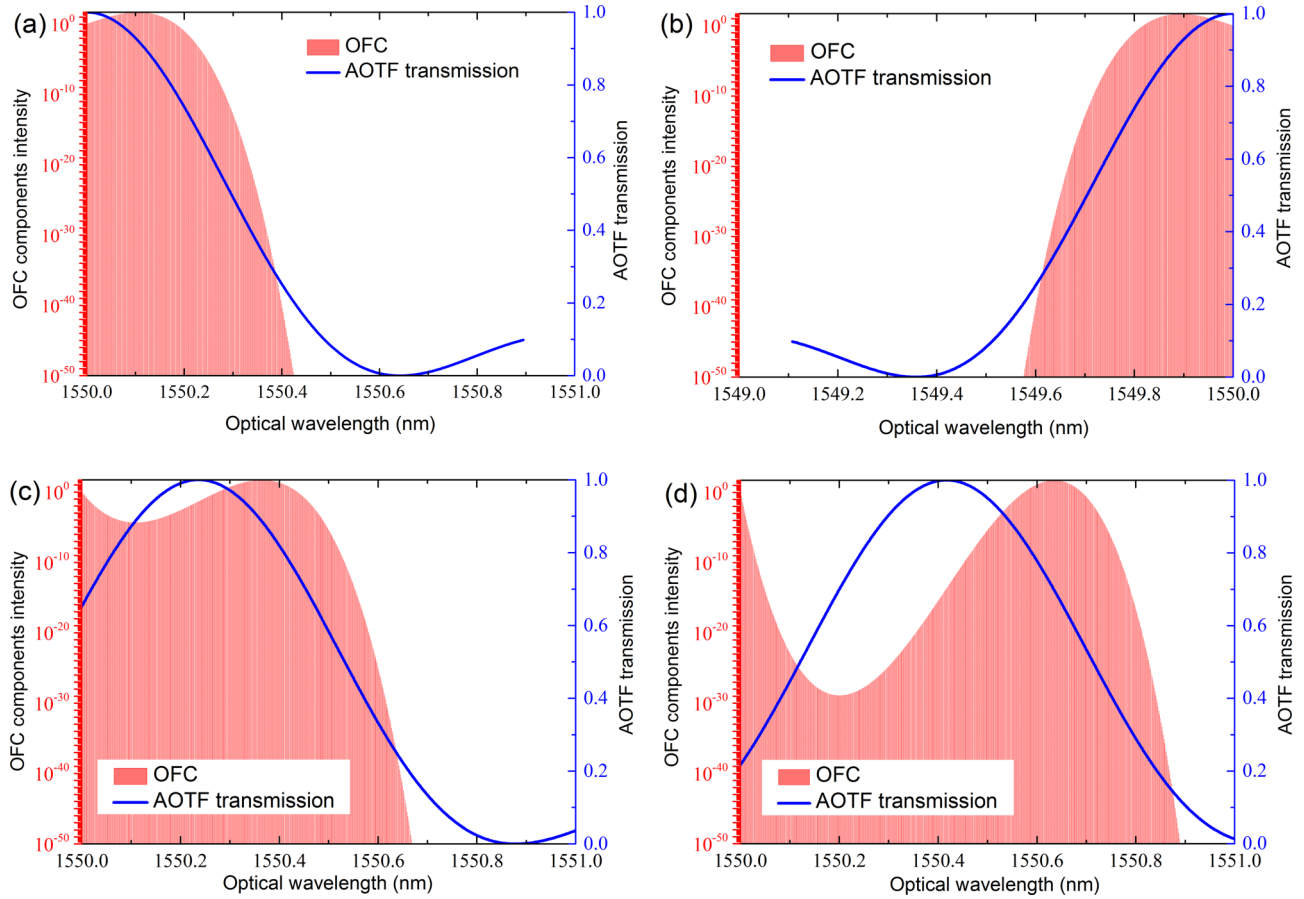

FIG. 8. Simulated OFC spectra and collinear AO cell transmission functions for varying mismatch generated with I_0 component: (a) $\alpha = 0°$, $\beta = 90°$, $\sigma = 2.98$, $R = 0, -1$ diffraction order; (b) $\alpha = 90°$, $\beta = 0°$, $\sigma = 2.98$, $R = 0, +1$ diffraction order; (c) $\alpha = 0°$, $\beta = 90°$, $\sigma = 3.03$, $R = -2$; (d) $\alpha = 0°$, $\beta = 90°$, $\sigma = 3.42$, $R = -3.5$

in Fig. 8(d). The total spectral width of the comb increases up to 0.9 nm and the number of spectral components is about 600. Thus, the mismatch between the seed wavelength and the rf signal can be used to increase the optical comb width.

Further transformations of the OFC shape with the mismatch increase occur as follows. The position of the maximum in the comb spectrum shifts to the right, the intensity of the components in the minimum decreases, and the number of components to the right of the minimum remains approximately the same.

The narrow spectral width of the optical combs in all cases is explained by high spectral selectivity of the AO cell. It is possible to increase the bandwidth reducing AO interaction length. For example, if we use the AO cell with $l = 0.5$ cm instead of 4 cm, the OFC spectral width will increase approximately by factor of 4. The important point is also that tuning the ultrasound frequency we are not only changing the width and the shape of the optical comb but also vary the interval between the spectral components of the comb. So one may tune all the parameters of the comb.

The next case to obtain OFC with SSB modulation is to apply I_1 component so that $\alpha = 0°$ and $\beta = 45°$ are chosen. In this case, the electromagnetic field after the polarizer contains two components and Eq. (16) transforms into:

$$\widetilde{E}_{\text{out}} = \widetilde{E}_0^Z \cos\beta + \widetilde{E}_{-1}^X \sin\beta. \tag{21}$$

According to Eq. (15), the terms obtain various phase shifts and the results of their interference depends on the number of passes through the optical feedback loop. The results of simulations for the SSB modulation with I_1 component are presented in Fig. 9.

The OFCs simulated for zero mismatch are shown in Figs. 9(a) and 9(b). These combs were obtained for polarizer orientation angles $\alpha = 0°$, $\beta = 45°$, and $\alpha = 90°$, $\beta = 45°$ corresponding to -1st and $+1$st diffraction orders respectively. In all the cases $\Gamma = \pi/2$.

Unlike the SSB modulation with I_0 component, the combs for these two cases are not symmetrical. The reason of this difference is that the phase shifts between interfering components are not equal. For the same reason, the optical amplification coefficients vary. Figure 9(a) was simulated with $\sigma = 5.52$ and Fig. 9(b) with $\sigma = 4.18$. The OFC components intensity oscillations are also produced by phase shift periodically changing with number of passes. It is possible to reduce these oscillations by introducing the phase shift compensation with optical phase retarder mounted in the FSL. The comb shown in Fig. 9(a) contains approximately 280 components and has 0.4 nm spectral band, the OFC presented in Fig. 9(b) has only 160 components and 0.22 nm bandwidth.

The comb represented in Fig. 9(c) was simulated for nonzero mismatch $R = -1.8$ ($f = 185.94$ MHz) and $\sigma = 5.43$. As well as in the case of SSB modulation with I_0

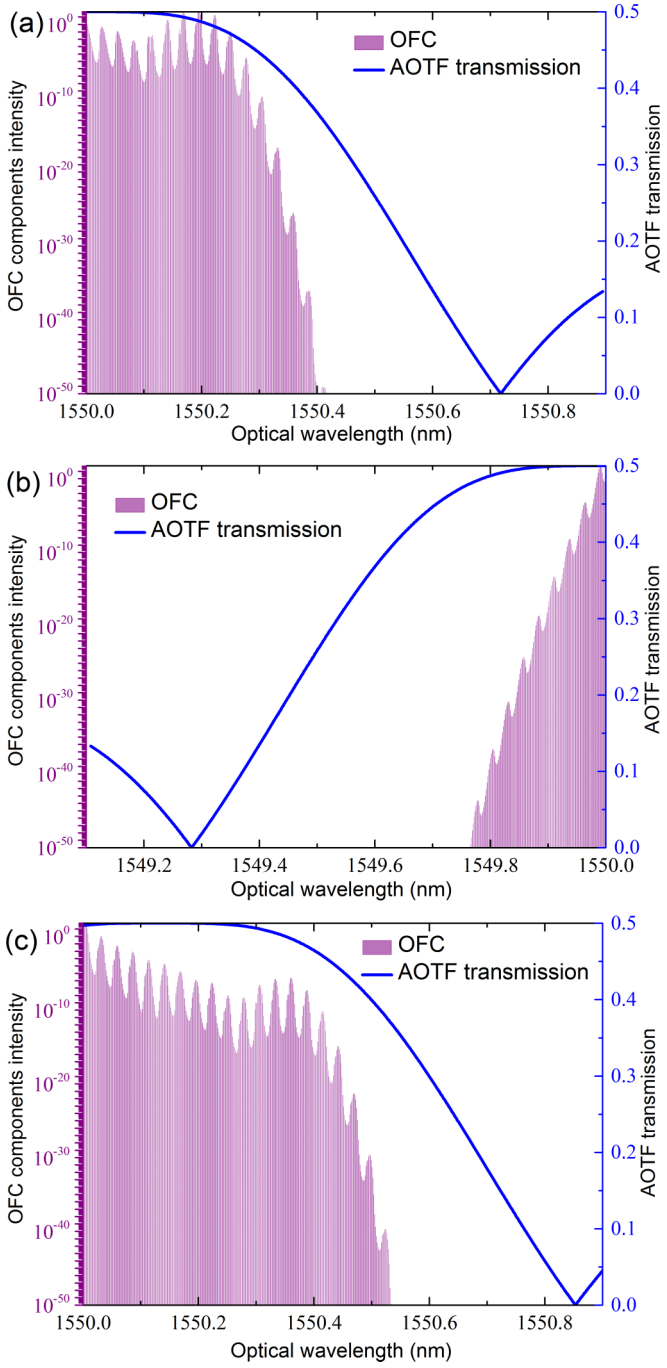

FIG. 9. Simulated OFC spectra and collinear AO cell transmission functions for varying mismatch generated with I_1 component: (a) $\alpha = 0°$, $\beta = 45°$, $\sigma = 5.52$, $R = 0, -1$ diffraction order; (b) $\alpha = 90°$, $\beta = 45°$, $\sigma = 4.18$, $R = 0, +1$ diffraction order; (c) $\alpha = 0°$, $\beta = 45°$, $\sigma = 5.43$, $R = -1.8$;

component, the mismatch growth causes the broadening of the OFC spectrum. In this case, the number of spectral components increases up to 360 and the optical band exceeds 0.46 nm.

The last case to obtain an equally spaced comb in the examined system is to apply I_2 component, setting $\alpha = \beta = 45°$. In this case, all four components $\widetilde{E}_0^Z$, $\widetilde{E}_{-1}^X$, $\widetilde{E}_0^X$, and $\widetilde{E}_{+1}^Z$ exist at the output of the AO filter and interfere with each other. Simulation results are presented in Fig. 10.

The OFC obtained for zero mismatch and $\sigma = 4.8$ is shown in Fig. 10(a). As it was described in Sec. III A [Fig. 5(b)], it has components with both shorter and longer wavelengths than the wavelength λ of the master oscillator. They are produced by $\widetilde{E}_{+1}^Z$ and $\widetilde{E}_{-1}^X$ correspondingly. The OFC has asymmetrical shape due to different phase shifts acquired by optical waves diffracted into -1st and $+1$st orders. The phase shift determines also to the presence of oscillation in the OFC spectrum. The comb contains 430 components and is as wide as 0.64 nm.

Figure 10(b) illustrates the case when the phase shift for $+1$st diffraction order is compensated with the optical beam retarder. It is possible to observe the oscillations suppression in the range of short optical wavelengths and the transformation of the OFC shape. Phase shift compensation also causes the reduction of required optical amplification. The OFC presented in Fig. 10(b) has the same maximal intensity as those presented in Fig. 10(a), but the optical amplification needed to generate it is $\sigma = 4.04$. The number of optical spectral components is approximately the same, but due to the phase delay compensation, the spectral band turns out to be shifted to 0.1 nm.

The OFCs presented in Figs. 10(c) and 10(d) were obtained for the same mismatch values but with opposite sign $R = \pm 2.1$. In this geometry (I_2 component), the mismatch growth also causes the appearance of the dip but the number spectral components in the comb reduces. The OFCs presented in Figs. 10(c) and 10(d) contain 300 and 240 lines, respectively. It is also possible to notice that the negative mismatches demand lower values of optical amplification than the positive ones $\sigma = 4.07$ for $R = 2.1$ and $\sigma = 3.67$ for $R = -2.1$.

Thus, we have studied three possible ways to obtain equally spaced OFCs in the examined system with optical only feedback. The changeover between the generation methods is implemented by changing the polarizers mutual orientation and HWP reorientation. The combs may be generated with two variants of SSB modulation (applying I_0 and I_1 components) and amplitude modulation (applying I_2 component). For SSB modulation, the number of spectral components increases with AO mismatch growth. The amplitude modulation gives the possibility to generate OFC with both shorter and longer wavelengths than the master oscillator has.

C. Chirped OFC generation

Chirped OFC generation can be achieved in the optical system with two feedback loops: an optical one and an electronic one (Fig. 4). The electric feedback loop has its own polarizer mounted after the beam splitter with the splitting ratio ϵ. Phenomenological model for this system was observed in Sec. III B. For this configuration of the OFC generator, we analyze only SSB modulation applying I_0 component since there is no optical phase shift that causes the oscillations of spectral components intensity and the OFC spectrum does not contain additional satellite components.

The seed radiation of the master oscillator is assumed to have only one spectral component with the wavelength

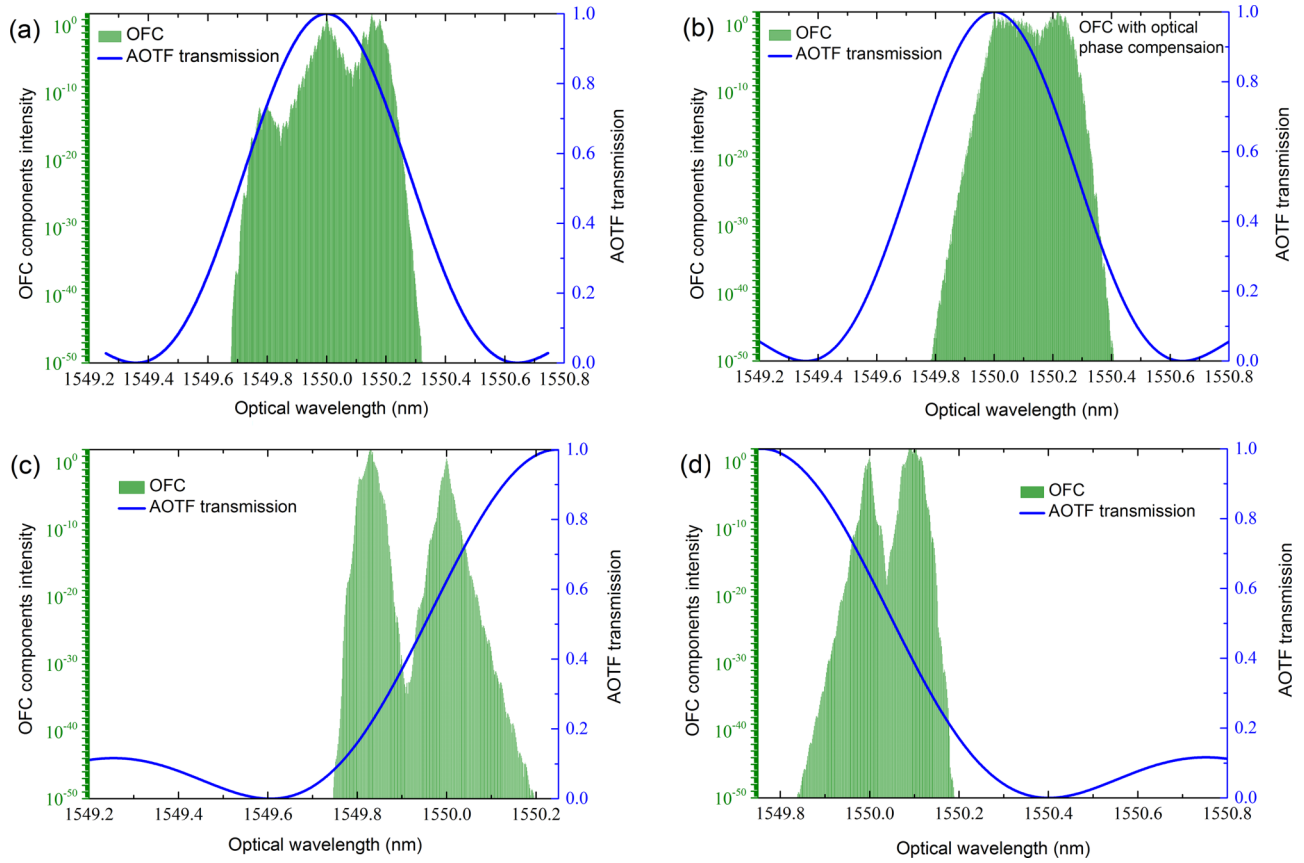

FIG. 10. Simulated OFC spectra generated with I_2 component and collinear AO cell transmission functions for varying mismatch ($\alpha = 45^\circ$, $\beta = 45^\circ$): (a) $\sigma = 4.8$, $R = 0$; (b) $\sigma = 4.04$, $R = 0$, with optical phase compensation; (c) $\sigma = 4.07$, $R = 2.1$; (d) $\sigma = 3.67$, $R = -2.1$

λ and normalized electromagnetic field at the system input is $\widetilde{E}_{\text{seed}} = 1$. The orientation of polarizers is chosen to be $\alpha = 0^\circ$ and $\beta = 90^\circ$. The polarizer in the electrical feedback arm is oriented at the angle $\gamma = 45^\circ$ to obtain the maximum magnitude of rf signal in the feedback circuit [60,61,67,68]. We assume that the gain in the electrical feedback is high enough for the system to operate in the generation mode [65,66]. Thus, the AO mismatch equals to zero for all optical spectrum components. In this case, the electromagnetic field at the optical feedback output after the first pass equals to:

$$\widetilde{E}_{\text{out}} = \upsilon(1-\chi)\sigma\epsilon\widetilde{E}_{\text{seed}} \sin\frac{\Gamma_1}{2} \exp(-jk_e l)\delta(\omega-\omega_1), \tag{22}$$

where Γ_1 is the Raman-Nath parameter for seed light with wavelength λ and normalized intensity $I_{\text{seed}} = 1$. Calculation of the Γ_1 value is based on the conditions of the amplitude and phase balance for the electric feedback circuit in the approximation of the low diffraction efficiency [65,66]. In this system, the balance conditions are determined by the equation:

$$\Gamma_1 = \frac{\rho\kappa\psi\nu(1-\epsilon)I_{\text{i}}}{2} \sin\Gamma_1, \tag{23}$$

where ρ is the detector sensitivity, κ is the electric feedback gain, ψ the AO cell transducer efficiency, I_{i} is the intensity of the optical radiation spectral component. An acoustic wave is excited in AO cell only if condition (23) is satisfied. The threshold value of the gain factor κ when oscillations emerge in the electrical feedback circuit for mth spectral component with I_{im} intensity is

$$\kappa = \frac{2}{\rho\psi\nu(1-\epsilon)I_{im}}. \tag{24}$$

After N passes through the optical feedback circuit under the condition of the amplitude balance for each of the spectral component, the intensity at the output of the optical feedback will be defined as:

$$\widetilde{E}_N = \widetilde{E}_{\text{seed}} \sum_{n=1}^{N} [\upsilon\epsilon(1-\chi)\sigma]^n \prod_{m=1}^{n} \sin\left(\frac{\Gamma_m}{2}\right), \tag{25}$$

where Γ_m is

$$\Gamma_m = \widetilde{E}_{\text{seed}}[\upsilon\epsilon(1-\chi)\sigma]^{m-1} \times \prod_{m=2}^{n} \sin\left(\frac{\Gamma_{m-1}}{2}\right) \frac{\rho\kappa\psi\nu(1-\epsilon)}{2} \sin\Gamma_m. \tag{26}$$

The OFC spectral components' wavelengths are defined by Eq. (11). Equations (25) and (26) can be used to simulate the chirped OFCs. We have chosen the following parameters for the simulations: $\nu = 0.5$, $\chi = 0.3$, $\epsilon = 0.7$, $\psi = 0.9$, and $\rho = 0.7$. The gain coefficients of electric feedback κ and of optical loop σ were varied in such a way as to get the widest possible comb. The coefficient κ must also exceed the threshold value Eq. (24). This value depends on the intensity of light radiation,

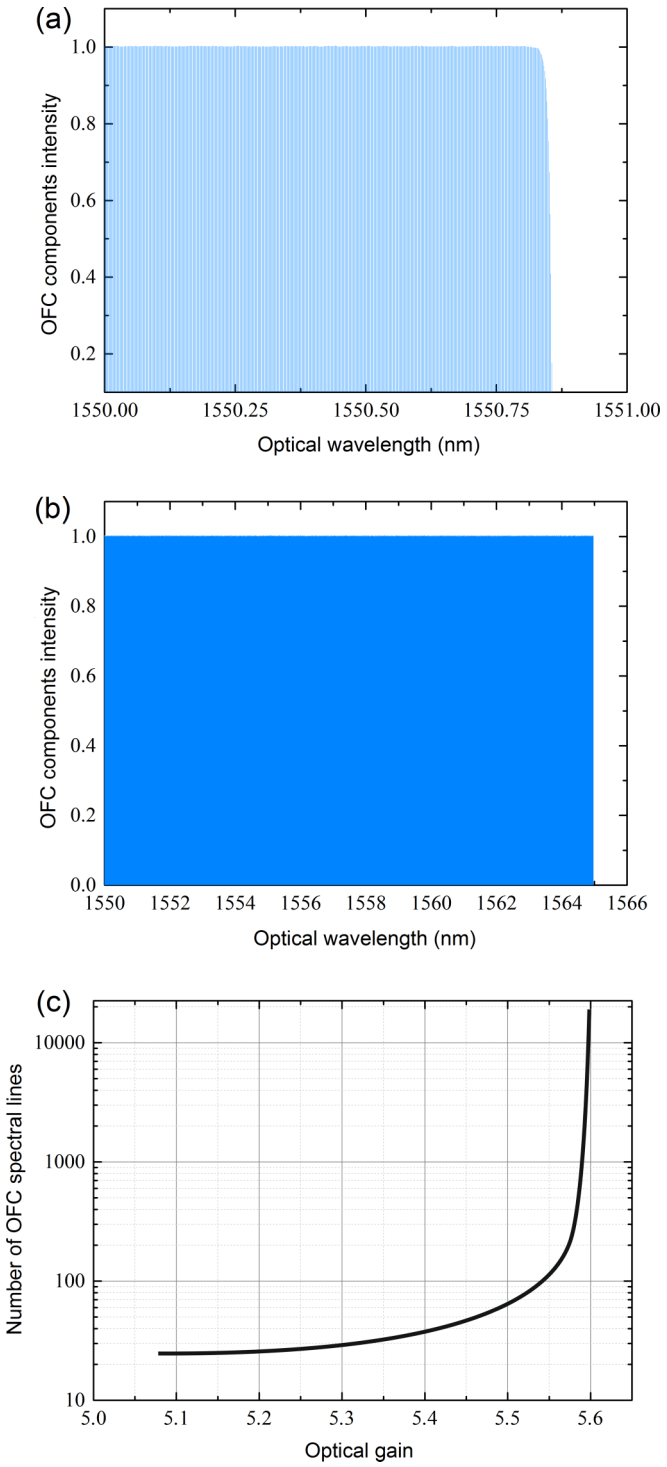

FIG. 11. Simulated chirped OFC spectra obtained with SSB modulation for (a) $\sigma = 5.59$ and (b) $\sigma = 5.60$ and simulated dependence of number of OFC spectrum lines on the optical gain σ.

which, in turn, depends on the gain of the optical feedback circuit.

Figures 11(a) and 11(b) represent the results of OFC spectra simulations made for $\kappa = 35$ and two values of optical feedback gain factors $\sigma = 5.59$ for and $\sigma = 5.60$. The calculations were carried out for the case when the system parameters, first of all, detector sensitivity and transducer efficiency, do not depend on the wavelength of optical radiation and rf frequency. For the presented spectral range this assumption is correct as the characteristics of all optical and electrical elements of the system does not change significantly in this band. In the case shown in Fig. 11(a), the gain of the optical feedback circuit is not sufficient to create a broad optical comb. The OFC shown in Fig. 11(a) contains only about 580 spectral lines.

By increasing the optical gain (from $\sigma = 5.59$ to $\sigma = 5.60$), it is possible to obtain a much wider comb. The spectral width of the comb is not limited by the new frequency components synthesis mechanism and AO filter transmission function width. First of all, it is limited by the system parameters (optical gain, polarizer and HWP properties, and others) depending on the optical radiation wavelength and also by the parameters the electrical feedback circuit depending on the radio signal frequency. The OFC spectrum shown in Fig. 11(b), contains $\sim 10^4$ spectral lines and this is only the part of the obtained OFC. As the comb is chirped, the spectral interval $\Delta\lambda_N$ between the adjacent components increases in the presented band from 1.490×10^{-3} nm to 1.503×10^{-3} nm (from 185.927 MHz–187.549 MHz).

The simulation of the dependence of the spectral lines number in OFC on the optical gain σ carried also for the ideal case is shown in Fig. 11(c). The number of the OFC components exhibits exponential-like dependence on the optical gain. The optical gain increasing from 5.1 to 5.6 causes the growth of spectral lines amount from 25 to more than $\sim 10^4$.

In reality, the AO cell may have approximately the same efficiency in the octave spanning wavelength range [69]. Thus, this system with optical and electric feedback in ideal case allows to obtain optical combs as wide as the optical tuning range of the AO cell but the width of real OFC will be limited by the spectral characteristics of the other elements in the proposed scheme such as optical amplifier, photodetector, electric signal phase shifter. It should be mentioned that the OFC represents the short optical pulse train only in some particular cases. In the described system, the optical phase of each OFC line is fixed and strictly defined by the phase delays in the optical path. This phase dependence on OFC line number may be controlled by commercially available phase shifters or can be easily compensated with a piece of standard optical dispersive fiber in order to convert OFC to short pulse train in the time domain.

V. SUMMARY

In this paper, we have examined the possibilities of OFC generation with collinear AO interaction and proposed two optoelectronic systems. The first one contains only the optical FSL feedback and the second one contains also the electronic feedback loop. It is shown that several OFC generation methods may be applied in these systems. The generation method transition in both systems is realized simply by mutual orientation of the polarizers and the HWP in the feedback loops.

The examination of the closed-loop optical system has shown that the shape of OFC depends on the AO mismatch being set by the rf generator frequency. The most effective

way to obtain the OFC in this system is the SSB modulation with crossed polarizers. The spectral interval between the OFC components is defined by the rf generator frequency also. The OFC band in this system is determined mainly by the spectral selectivity of the collinear AO filter. The OFC spectrum can be broadened using the phase mismatch between the seed laser wavelength and the rf signal applied to the AO filter.

The optoelectronic system with both optical and electronic feedback loops operates like the AO generator and does not require the external rf generator. It is possible to obtain OFCs in such system by several ways also. In this system, due to the electronic feedback, the spectral selectivity of the AO cell does not influence on the OFC band as the phase-matching condition is fulfilled for all spectral components of light radiation and they are diffracted in the AO cell independently by different spectral components of the acoustic wave. Due to the dependence of AO interaction phase-matching frequency on the optical wavelength the spectral interval between OFC components in this system is chirped.

The study of possible OFC generation ways has shown that the most effective is SSB modulation with crossed polarizers. In this case, the OFC can be obtained in a wide spectral band determined by the spectral characteristics of the photodetector used in the electronic feedback and the AO parameters.

The presented AO methods of OFC generation in a FSL scheme can be applied in the entire optical range of the AO devices operation (from UV to middle IR). The operation at shorter optical wavelengths is even more preferable as the AO devices are more effective in this range. In a general case, the spectral interval between OFC components is defined by the AO phase-matching frequency that depends on the AO cell material and AO interaction geometry. Thus the examined systems offer significant opportunities for OFC generation.

ACKNOWLEDGMENTS

This paper was supported by grants of the Ministry of Education and Science of the Russian Federation (Project 02.A03.21.0004) and Russian Foundation for Basic Research (Project No. 17-02-00522); the development of mathematical model and simulations presented in Secs. III and IV were supported by Russian Science Foundation (Project No. 18-72-00036).

[1] S. T. Cundiff and J. Ye, Rev. Mod. Phys. **75**, 325 (2003).
[2] N. R. Newbury, Nature Photon. **5**, 186 (2011).
[3] P. Marin-Palomo, J. N. Kemal, M. Karpov, A. Kordts, J. Pfeifle, M. H. P. Pfeiffer, P. Trocha, S. Wolf, V. Brasch, M. H. Anderson *et al.*, Nature (London) **546**, 274 (2017).
[4] T. Ideguchi, S. Holzner, B. Bernhardt, G. Guelachvili, N. Picqué, and T. W. Hänsch, Nature (London) **502**, 355 (2013).
[5] I. Coddington, W. C. Swann, L. Nenadovic, and N. R. Newbury, Nature Photon. **3**, 351 (2009).
[6] I. Coddington, N. Newbury, and W. Swann, Optica **3**, 414 (2016).
[7] S. A. Diddams, T. Udem, J. C. Bergquist, E. A. Curtis, R. E. Drullinger, L. Hollberg, W. M. Itano, W. D. Lee, C. W. Oates, K. R. Vogel *et al.*, Science **293**, 825 (2001).
[8] N. Hinkley, J. A. Sherman, N. B. Phillips, M. Schioppo, N. D. Lemke, K. Beloy, M. Pizzocaro, C. W. Oates, and A. D. Ludlow, Science **341**, 1215 (2013).
[9] R. A. McCracken, J. M. Charsley, and D. T. Reid, Opt. Express **25**, 15058 (2017).
[10] J. Mizrahi, B. Neyenhuis, K. G. Johnson, W. C. Campbell, C. Senko, D. Hayes, and C. Monroe, Appl. Phys. B **114**, 45 (2014).
[11] A. Schliesser, N. Picqué, and T. W. Hänsch, Nature Photon. **6**, 440 (2012).
[12] S. B. Papp, K. Beha, P. Del'Haye, F. Quinlan, H. Lee, K. J. Vahala, and S. A. Diddams, Optica **1**, 10 (2014).
[13] G. Porat, C. M. Heyl, S. B. Schoun, C. Benko, N. Dörre, K. L. Corwin, and J. Ye, Nature Photon. **12**, 387 (2018).
[14] T. Ohara, H. Takara, T. Yamamoto, H. Masuda, T. Morioka, M. Abe, and H. Takahashi, J. Lightwave Technol. **24**, 2311 (2006).
[15] P. Del'Haye, A. Schliesser, O. Arcizet, T. Wilken, R. Holzwarth, and T. J. Kippenberg, Nature (London) **450**, 1214 (2007).
[16] T. Herr, V. Brasch, J. D. Jost, C. Y. Wang, N. M. Kondratiev, M. L. Gorodetsky, and T. J. Kippenberg, Nature Photon. **8**, 145 (2014).
[17] A. V. Cherenkov, V. E. Lobanov, and M. L. Gorodetsky, Phys. Rev. A **95**, 033810 (2017).
[18] N. G. Pavlov, S. Koptyaev, G. V. Lihachev, A. S. Voloshin, A. S. Gorodnitskiy, M. V. Ryabko, S. V. Polonsky, and M. L. Gorodetsky, Nature Photon. **12**, 694 (2018).
[19] A. S. Raja, A. S. Voloshin, H. Guo, S. E. Agafonova, J. Liu, A. S. Gorodnitskiy, M. Karpov, N. G. Pavlov, E. Lucas, R. R. Galiev *et al.*, Nature Commun. **10**, 680 (2019).
[20] M.-G. Suh and K. Vahala, Optica **5**, 65 (2018).
[21] T. J. Kippenberg, A. L. Gaeta, M. Lipson, and M. L. Gorodetsky, Science **361**, eaan8083 (2018).
[22] O. A. Egorov and D. V. Skryabin, Opt. Express **26**, 24003 (2018).
[23] A. Villois and D. V. Skryabin, Opt. Express **27**, 7098 (2019).
[24] M. Dong, S. T. Cundiff, and H. G. Winful, Phys. Rev. A **97**, 053822 (2018).
[25] M. Bagheri, C. Frez, L. A. Sterczewski, I. Gruidin, M. Fradet, I. Vurgaftman, C. L. Canedy, W. W. Bewley, C. D. Merritt, C. S. Kim *et al.*, Sci. Rep. **8**, 3322 (2018).
[26] J. Li, Y. Qu, R. Yu, and Y. Wu, Phys. Rev. A **97**, 023826 (2018).
[27] M. Stefszky, V. Ulvila, Z. Abdallah, C. Silberhorn, and M. Vainio, Phys. Rev. A **98**, 053850 (2018).
[28] J. Li, S. Shen, Y. Qu, D. Zhang, and Y. Wu, Phys. Rev. A **98**, 023848 (2018).
[29] B. Jerez, P. Martín-Mateos, E. Prior, C. de Dios, and P. Acedo, Opt. Lett. **41**, 4293 (2016).
[30] B. Jerez, P. Martín-Mateos, E. Prior, C. de Dios, and P. Acedo, Opt. Express **24**, 14986 (2016).
[31] P. Coppin and T. G. Hodgkinson, Electron. Lett. **26**, 28 (1990).

[32] S. Atutov, F. Bonazzi, R. Calabrese, V. Guidi, P. Lenisa, S. Petruio, E. Mariotti, and L. Moi, Opt. Commun. **132**, 269 (1996).
[33] J. Zhang, J. Yu, Z. Dong, Y. Shao, and N. Chi, Opt. Express **19**, 26370 (2011).
[34] H. Guillet de Chatellus, O. Jacquin, O. Hugon, W. Glastre, E. Lacot, and J. Marklof, Opt. Express **21**, 15065 (2013).
[35] V. Torres-Company and A. M. Weiner, Laser Photonics Rev. **8**, 368 (2013).
[36] H. Guillet de Chatellus, E. Lacot, W. Glastre, O. Jacquin, and O. Hugon, Phys. Rev. A **88**, 033828 (2013).
[37] H. Guillet de Chatellus, L. R. Cortés, and J. Azaña, Optica **3**, 1 (2016).
[38] C. Schnébelin and H. Guillet de Chatellus, Optica **4**, 907 (2017).
[39] J. Lamperski and P. Stepczak, Proc. SPIE **9816**, 981611 (2015).
[40] S. J. Herr, V. Brasch, J. Szabados, E. Obrzud, Y. Jia, S. Lecomte, K. Buse, I. Breunig, and T. Herr, Opt. Lett. **43**, 5745 (2018).
[41] F. Ferdous, D. E. Leaird, C.-B. Huang, and A. M. Weiner, Opt. Lett. **34**, 3875 (2009).
[42] D. A. Long, A. J. Fleisher, K. O. Douglass, S. E. Maxwell, K. Bielska, J. T. Hodges, and D. F. Plusquellic, Opt. Lett. **39**, 2688 (2014).
[43] P. Martín-Mateos, B. Jerez, and P. Acedo, Opt. Express **23**, 21149 (2015).
[44] G. Millot, S. Pitois, M. Yan, T. Hovhannisyan, A. Bendahmane, T. W. Hänsch, and N. Picqué, Nature Photon. **10**, 27 (2015).
[45] V. Durán, S. Tainta, and V. Torres-Company, Opt. Express **23**, 30557 (2015).
[46] V. Durán, C. Schnébelin, and H. Guillet de Chatellus, Opt. Express **26**, 13800 (2018).
[47] H. Guillet de Chatellus, L. R. Cortés, C. Schnébelin, M. Bwebsitea, and J. Azaña, Nature Commun. **9** (2018).
[48] V. I. Balakshy and S. N. Mantsevich, Opt. Laser Technol. **44**, 893 (2012).
[49] V. I. Balakshy and S. N. Mantsevich, Opt. Spectrosc. **106**, 441 (2009).
[50] V. I. Balakshy and S. N. Mantsevich, Tech. Phys. **56**, 1646 (2011).
[51] S. E. Harris and R. W. Wallace, J. Opt. Soc. Am. **59**, 744 (1969).
[52] S. E. Harris, S. T. K. Nieh, and R. S. Feigelson, Appl. Phys. Lett. **17**, 223 (1970).
[53] H. Gnewuch and C. N. Pannell, IEEE Trans. Ultrason. Ferroelectr. Freq. Control **49**, 1635 (2002).
[54] Yu. A. Zyuryukin, S. V. Zavarin, and A. N. Yulaev, Opt. Spectrosc. **107**, 152 (2009).
[55] A. Korpel, *Acousto-Optics* (Marcel Dekker, New York, 1988).
[56] V. I. Balakshy and S. N. Mantsevich, Opt. Spectrosc. **103**, 804 (2007).
[57] V. Ya. Molchanov and K. B. Yushkov, Opt. Express **22**, 15668 (2014).
[58] K. B. Yushkov and V. Ya. Molchanov, Opt. Commun. **355**, 177 (2015).
[59] K. B. Yushkov, V. Ya. Molchanov, A. V. Ovchinnikov, and O. V. Chefonov, Phys. Rev. A **96**, 043866 (2017).
[60] V. I. Balakshy, Yu. I. Kuznetsov, and S. N. Mantsevich, Quantum Electron. **46**, 181 (2016).
[61] S. N. Mantsevich, V. I. Balakshy, and Yu. I. Kuznetsov, Appl. Phys. B **123**, 101 (2017).
[62] S. P. Anikin, V. F. Esipov, V. Ya. Molchanov, A. M. Tatarnikov, and K. B. Yushkov, Opt. Spectrosc. **121**, 115 (2016).
[63] V. I. Balakshy and I. M. Sinev, Quantum Electron. **34**, 277 (2004).
[64] V. I. Balakshy and I. M. Sinev, J. Opt. A–Pure Appl. Opt. **6**, 469 (2004).
[65] S. N. Mantsevich and V. I. Balakshy, Appl. Phys. B **124**, 54 (2018).
[66] S. N. Mantsevich and V. I. Balakshy, J. Opt. Soc. Am. B **36**, 728 (2019).
[67] S. N. Mantsevich and V. I. Balakshy, IEEE Photonics J. **11**, 7800315 (2019).
[68] S. N. Mantsevich and V. I. Balakshy, J. Opt. Soc. Am. B **35**, 1030 (2018).
[69] V. Ya. Molchanov and O. Yu. Makarov, Opt. Eng. **38**, 1127 (1999).